tones are potentially important regions of differentiation and speciation that conceivably may enrich the biodiversity of tropical rainforests (9). Three observations lead to this conclusion. First, as we have shown for the little greenbul, divergent selection rather than drift or other factors has most likely caused morphologic differentiation in ecotone populations. Second, the magnitude of divergence in fitness-related characters is similar to that found between reproductively isolated species, which suggests that selection differences are large between ecotone and forest habitats. Third, laboratory experiments suggest that such divergent selection may sometimes lead to reproductive divergence. Our results suggest that ecotones may be integral to the production and maintenance of biodiversity in tropical rainforests. This contrasts with past theories of rainforest speciation that have focused on within-rainforest vicariance mechanisms (20). Currently, because ecotones may exhibit less species richness than central rainforest habitats, comparatively less attention is paid to conserving them. If further research supports the role of ecotones as centers for speciation, their dynamics will need to be preserved so that rainforest biodiversity can be sustained and replenished.

REFERENCES AND NOTES

1. M. Slatkin, *Science* **236**, 787 (1987).
2. J. A. Endler, *Geographic Variation, Speciation, and Clines*, (Monogr. Popul. Biol. 10, Princeton Univ. Press, Princeton, NJ, 1977).
3. A. R. Templeton, *Evolution* **41**, 233 (1987); E. Mayr, *Animal Species and Evolution* (Harvard Univ. Press, Cambridge, MA, 1963).
4. R. R. Rice and E. E. Hostert, *Evolution* **47**, 1637 (1993).
5. A. C. Millington, P. J. Styles, R. W. Critchley, in *Nature and Dynamics of Forest-Savanna Boundaries*, P. A. Furley, J. Proctor, J. A. Ratter, Eds. (Chapman and Hall, New York, 1992), pp. 37–62.
6. K. A. Longman and J. Jenik, *ibid.*, pp. 3–20.
7. T. B. Smith, *Nature* **363**, 618 (1993).
8. J. P. Chapin, *Bull. Am. Mus. Nat. Hist.* **75**, 1 (1954).
9. J. A. Endler, *Am. Zool.* **22**, 441 (1982); in *Biological Diversification in the Tropics*, G. T. Prance, Ed. (Columbia Univ. Press, New York, 1982), pp. 641–657.
10. B. P. Hall and R. E. Moreau, *An Atlas of Speciation in African Passerine Birds* (British Museum, London, 1970); T. M. Crowe and A. A. Crowe, *J. Zool. London* **198**, 417 (1982); J. P. Chapin, *Bull. Am. Mus. Nat. Hist.* **65**, 1 (1932).
11. The number, location, and dates of field work for each forest site were as follows: 1, Kribi (2°43′N, 9°52′E), 6 to 9 October 1990 and 1 to 4 July 1993; 2, Ndibi (3°46′N, 12°12′E), 28 July to 20 October 1990; 3, Zoebefame (2°39′N, 13°23′E), 27 to 29 September 1990 and 9 to 15 June 1993; 4, Bobo Camp (2°39′N, 13°28′E) 15 to 20 June 1993; 5, Nkwouak (3°52′N, 13°18′E), 7 to 8 August 1990 and 29 June to 2 July 1993; and 6, Lac Lobeke (2°18′N, 15°45′E), 25 to 29 June 1993. Those for each ecotone site were as follows: 7, Tibati (6°30′N, 12°35′E), 26 to 29 August 1990 and 5 to 10 July 1995; 8, Ngaoundaba Ranch (7°08′N, 13°41′E), 19 to 23 May 1995; 9, Wakwa, (7°16′N, 13°31′E), 21 to 23 August 1990 and 29 June to 4 July 1995; 10, Bétaré Oya (5°34′N, 14°05′E), 11 to 13 August 1990 and 5 to 8 May 1995; 11, Meiganga (6°31′N, 14°18′E), 15 to 19 August 1990 and 10 to 14 May 1995; and 12, Djohong (6°50′N, 14°42′E), 15 to 17 May 1995.
12. P. T. Boag and A. van Noordwijk, in *Avian Genetics: A Population and Ecological Approach*, F. Cooke and P. A. Buckley, Eds. (Academic Press, New York, 1987), pp. 45–78.
13. B. R. Grant and P. R. Grant, *Proc. R. Soc. London Ser. B Biol. Sci.* **251**, 111 (1993); T. B. Smith, *Evolution* **44**, 832 (1990); D. Schluter and J. N. M. Smith, *ibid.* **40**, 221 (1986); D. Schluter, *Ecol. Monogr.* **58**, 229 (1988).
14. C. W. Benkman, *Evol. Ecol.* **5**, 118 (1991).
15. S. Wright, *Evolution and the Genetics of Populations* (Univ. of Chicago Press, Chicago, IL, 1968), vol. 1.
16. M. Nei, *Molecular Evolutionary Genetics* (Columbia Univ. Press, New York, 1987).
17. D. B. Goldstein, A. Ruiz Linares, L. L. Cavalli-Sforza, M. W. Feldman, *Genetics* **139**, 463 (1995); M. Slatkin, *ibid.*, p. 457.
18. C. L. Tarr, *Mol. Ecol.* **4**, 527 (1995).
19. Ecotone-forest differences are greater than a third of the interspecific differences in wing length and a fifth of those in mass. When between-species differences in tarsus length, upper mandible length, and weight were contrasted by means of principal components analysis, the results were similar. Using the difference in mean character size between species and between ecotone and forest populations of *A. virens*, we calculated principal components using a correlation matrix. Forest-ecotone comparisons of *A. virens* were greater than 2 and 11 of the interspecific comparisons, along PC1 and PC2, respectively.
20. E. Mayr and R. J. O'Hara, *Evolution* **40**, 55 (1986); J. Haffer, *Science* **165**, 131 (1969).
21. R. Letouzey, *Etude Phytogeographique du Cameroun*, vol. 69 of *Encyclopedie Biologie* (Lechevalier, Paris, 1968).
22. S. Keith, E. K. Urban, C. H. Fry, *The Birds of Africa* (Academic Press, New York, 1992), vol. 4.

23. We thank the government of the Republic of Cameroon for permission to conduct the field research; J. Endler, M. Kirkpatrick, S. MacLane, C. Mortiz, M. Orr, S. Palumbi, E. Routman, C. Schneider, M. Slatkin, M. Turelli, B. Van Valkenburgh, and J. Carothers for helpful discussion and comments; and B. Larison, D. McNiven, R. Fotso, K. Whitney, M. Kimura, M. Fogiel, T. Robson, R. Zebell, and E. Taylor for assistance with field and laboratory work. The research was supported by the National Geographic Society, NERC grant GR3/8551′A′, the World Wildlife Fund, Royal Society grant 571310.V703, and NSF grant BSR 88-17336.

27 January 1997; accepted 18 April 1997

Macrophages as a Source of HIV During Opportunistic Infections

Jan M. Orenstein,* Cecil Fox, Sharon M. Wahl

The source of increasing viremia that characterizes the latter stages of human immunodeficiency virus (HIV) disease has remained a paradox because it occurs at a time when lymphoid tissue is quantitatively and qualitatively impaired, and the patients' CD4 T lymphocytes are steadily declining. Here, macrophages, both infected and uninfected with common opportunistic pathogens of HIV disease such as *Mycobacterium avium* complex and *Pneumocystis carinii*, were identified as highly productive sources of HIV in coinfected lymph nodes. These observations indicate that tissue macrophages are not only infected with HIV, but that common pathogens of HIV disease can dramatically increase their production of virus. Thus, prevention or successful treatment of opportunistic coinfections, or both, potentially benefits the patient twofold by limiting the pathology caused by opportunistic infection and by controlling induction of HIV replication.

Opportunistic infections (OIs) and rising levels of circulating human immunodeficiency virus–type 1 (HIV-1) are hallmarks of progressing HIV-1 disease (*1*). After infection with HIV-1, a variably paced loss of CD4 T lymphocytes leads to immunodeficiency and increasing susceptibility to a broad range of opportunistic viral, bacterial, fungal, and protozoal pathogens. A direct correlation between OIs and HIV-1 expression in vitro is paralleled by emerging in vivo evidence (*2*). Infections with common opportunistic pathogens, such as herpesvirus type-1, *Mycobacterium avium* complex, and *M. tuberculosis* are accompanied by mostly reversible increases in HIV-1 viremia (*2–4*). Bacterial pneumonia, an increasing cause of morbidity and mortality in HIV-1 infection, is also associated with increased circulating HIV-1 (*5*).

The source of the increased circulating HIV-1 has remained a puzzle because progression of HIV-1 disease is also characterized by involution of lymphoid tissue. Lymph nodes characteristically display progressive loss of germinal centers, leaving little if any remaining follicular dendritic cell–associated virus and only scattered productively infected $CD4^+$ lymphocytes. The role of the long-lived, mobile phagocyte as a source of virus during HIV-1 disease has been considered minimal, as few if any productively infected cells expressing monocyte/macrophage

J. M. Orenstein, Department of Pathology, George Washington University, Washington, DC 20037, USA.
C. Fox, Molecular Histology Inc., Gaithersburg, MD 20879, USA.
S. M. Wahl, Oral Infection and Immunity Branch, National Institute of Dental Research, National Institutes of Health, Bethesda, MD 20892, USA.

*To whom correspondence should be addressed. E-mail: jmo@gwis2.circ.gwu.edu

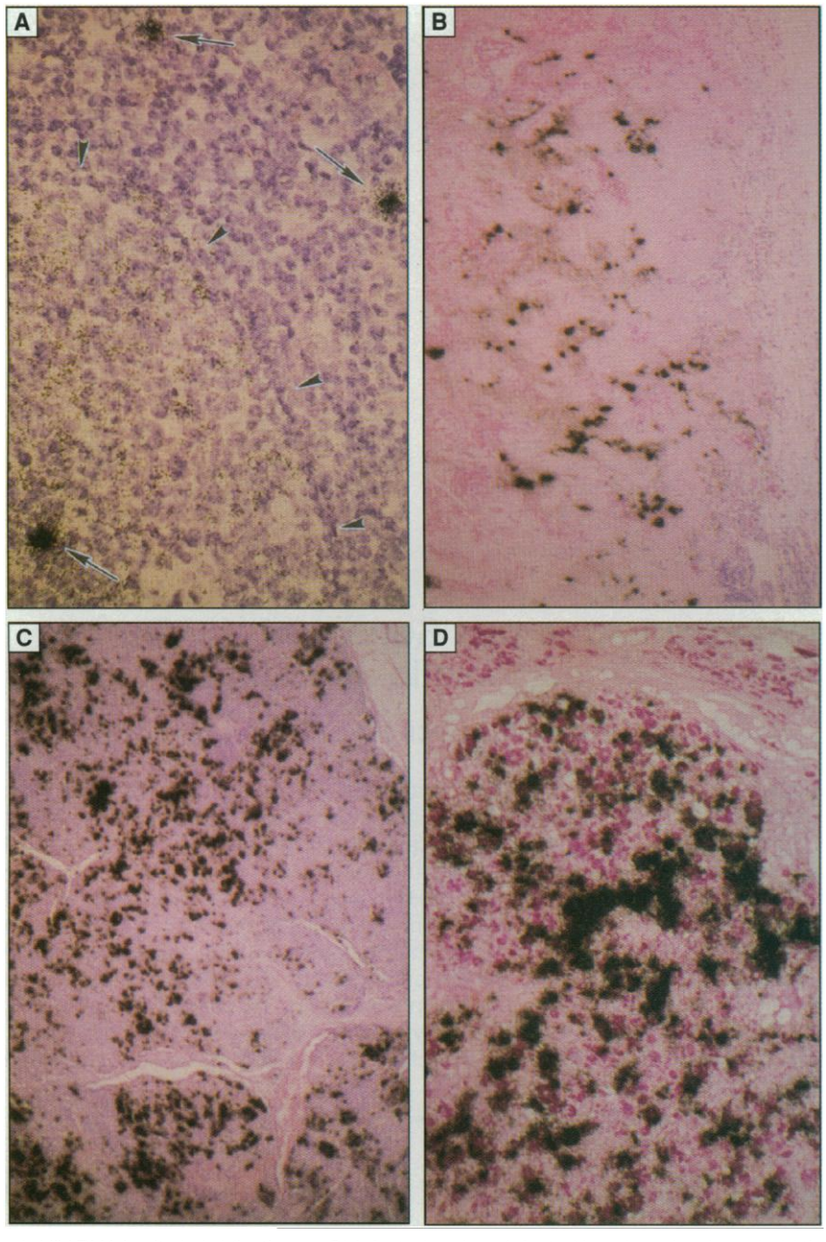

Fig. 1. HIV RNA in situ hybridization on OI-infected and noninfected lymph nodes. Lymphoid tissues from HIV-1–infected individuals, obtained surgically at the George Washington University Medical Center, Washington, D.C., were fixed in 10% neutral buffered formalin, embedded in paraffin, sectioned, and processed for in situ hybridization. For identification of HIV-1, protease-treated and untreated tissue sections (6 μm) (*7*) were hybridized to ^{35}S- or ^{33}P-labeled antisense RNA representing 9 kb of the HIV-1 genome (IIIB) to detect the presence of HIV-1 viral RNA. Both sense (control) and antisense probes were used. After hybridization, the slides were dipped in NTB 2 Kodak emulsion, exposed over dessicant for 4 days at 4°C, and developed in D-19 at 15°C for 4 min. (**A**) In an HIV-positive, OI-negative, hyperplastic lymph node, protease pretreatment was necessary to reveal the bulk of the HIV-1 RNA (black grains) which was associated with the cytoplasmic processes of FDC in germinal centers (arrowheads). Scattered HIV-positive lymphocytes were seen around and within germinal centers (arrows). The linear FDC-associated signal is difficult to discern with bright-field optics below this magnification (original magnification, ×400). (**B** and **C**) In marked contrast, the intensity of the HIV-1 signal was so pronounced in the PC- and MAC-infected node specimens that it was readily visible at original magnifications of ×60 (B) and ×40 (C), respectively. The nodal architecture was disrupted, lymphocytes were depleted, and dense and diffuse collections of HIV-1 signal were prominent (black grains). The ISH grains were especially concentrated over cells but were also seen in adjacent acellular areas. (**D**) In the MAC-infected lymph node, the HIV signal coincided with mononuclear and especially, multinucleated phagocytes rich in internalized acid-fast (red) MAC bacilli. The tissues were first hybridized and developed, and acid-fast Kinyoun's staining was performed on the emulsion-coated slides (original magnification, ×160).

markers have been documented either in the circulation or in lymphoid tissue (6–8). However, $CD4^+$ macrophages are productively infected in the central nervous system of patients with acquired immunodeficiency syndrome (AIDS) dementia complex and vacuolar myelopathy (8). Furthermore, their numbers are maintained in HIV-1 disease and, both in vitro and in vivo, monocyte/macrophages have

Table 1. HIV-1–expressing cells in lymph nodes with and without opportunistic infections. Excisional biopsies were obtained with consent from 10 males, aged 28 to 50, and one 33-year-old female with AIDS-defining opportunistic infections (OIs) and from 67 HIV-1 seropositive subjects without evidence of OIs. Tissue sections were processed without and with (shown) protease and in situ hybridization using HIV-1 sense and antisense probes performed as described (*7*). After in situ hybridization, the entire tissue sections were imaged with a CCD camera and 60-mm macro lens. Using NIH Image and a Macintosh 8100/80AV computer, the areas of the sections were determined by planimetry based on a 10-mm bar standard. Subsequently, HIV-1 expressing mononuclear cells (not FDC associated HIV) in the entire tissue sections were counted in a darkfield microscope at a numerical aperture of 0.32. Positive cells were considered to have more than 20 silver grains per 200 μm^2 and were expressed as the number of productively infected cells per 10 mm^2 of lymph node tissue. Most of the cells in the OI-infected tissues had far more than this number of grains directly over the cell, making it impossible to quantitate their numbers. Cell numbers in highly infected tissues represent underestimates due to giant cells, the presence of multiple cell aggregation, and intense positivity of signal. MAC, *Mycobacterium avium* complex; MK, *Mycobacterium kansasii*; PC, *Pneumocystis carinii*; MTB, *Mycobacterium tuberculosis*; Histo, *Histoplasma capsulatum*.

Patient	OI	HIV-1+ cells per 10 mm^2
AIDS		
1	MAC	13.6
2	MAC	55.2
3	MAC	12.6
4	MAC	84.1
5	MAC	176.6
6	MAC	11.4
7	Histo	26.3
8	MK	29.0
9	MK	0.8
10	PC	118.8
11	MTB	54.6
*Non-AIDS**		
Follicular hyperplasia (n = 24)	None	2.8
Hyperplasia/involution (n = 21)	None	1.4
Follicular involution (n = 18)	None	2.0
Lymphocyte depleted (n = 4)	None	0.5

*Non-AIDS tissues include specimens and unpublished data from the Division of AIDS Treatment Research Initiative Study 003.

been shown, unlike lymphocytes, to be capable of producing large amounts of both intracellular and extracellular HIV-1 without necessarily succumbing to the lethal effects of productive viral infection. To resolve the inconsistency of enhanced HIV-1 replication despite decreasing $CD4^+$ T cells, we focused on the potential role of the macrophage.

Probing of two *Pneumocystis carinii* (PC)–infected lymph nodes, excised from a patient with disseminated disease (9), by HIV-1 RNA in situ hybridization (ISH) for HIV-1–specific RNA revealed marked amounts of virus. The HIV-1–positive cells in these specimens far exceeded the number of productively infected lymphocytes characteristic of typical OI-free, hyperplastic lymph nodes from HIV-1–infected patients (Fig. 1, A and B). The PC lymph node specimens were almost totally replaced by necrotizing, hemorrhagic PC infection with only small amounts of residual lymphoid tissue (Fig. 1B). Whereas HIV-1 RNA expression was especially associated with collections of inflammatory cells within the OI, it was also present in apparently cell-free areas (Fig. 1B). In non-OI infected lymph nodes, the bulk of the HIV-1 signal was characteristically associated with follicular dendritic cell (FDC) processes as virus: complement–antibody complexes and was by far best observed when ISH was performed after predigestion of the tissue sections with protease, which enhances penetration of the probe (Fig. 1A) (7). After protease and ISH, FDC-entrapped HIV was seen as a linear display of grains along myriad FDC processes, and productively infected cells were distinguished by the superimposition of the signal over the cell in a "starburst"-like image. In contrast, protease pretreatment neither substantially increased the number of HIV-1 RNA–positive cells nor the amount of signal in the PC co-infected lymph nodes, and did not reveal areas of residual FDC-associated HIV-1 (Fig. 1B). Rather, HIV-1 signal was demonstrated to be very intense both with or without protease digestion and to be associated with mononuclear and multinucleated cells.

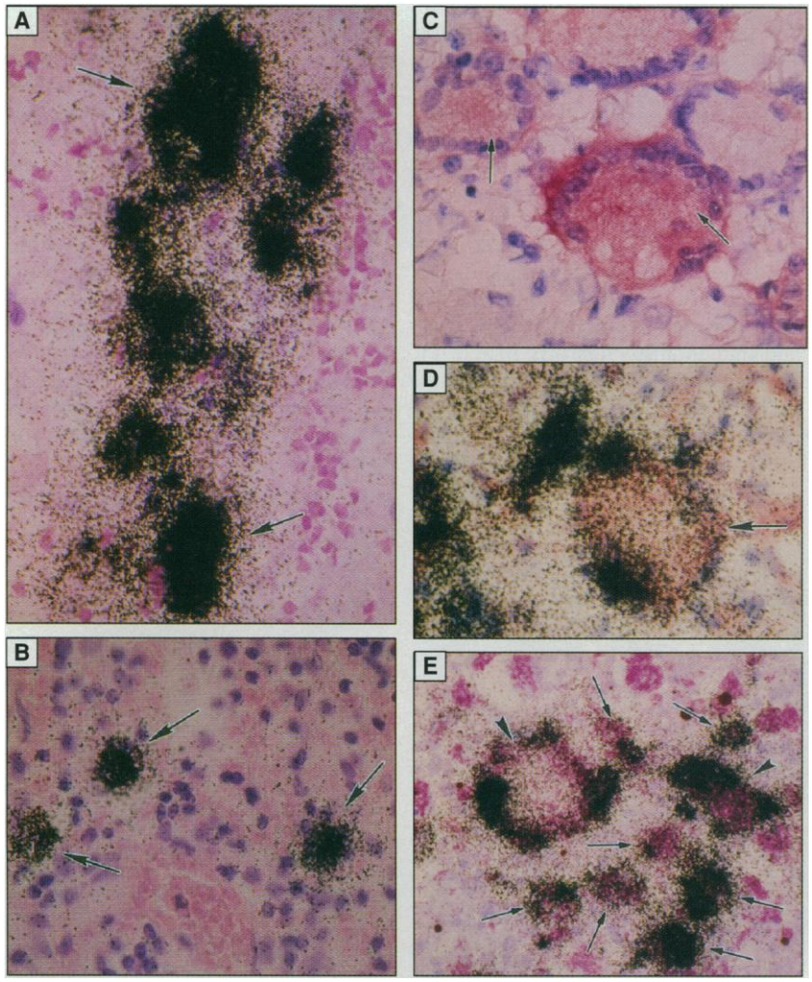

Fig. 2. Macrophages as the source of the HIV-1 RNA. (**A**) Collection of HIV-1–positive macrophages (cells obscured by grains; arrows indicate two of these) surrounded by erythrocytes in a PC-infected node. Original magnifications for (A) through (D) are ×640. (**B**) Typical starburst images of HIV-1–expressing lymphocytes (arrows) in the PC-infected node. (**C**) HIV p24–positive (red stain) MAC-infected multinucleated Langhans'-type giant cells. The clear needle-like intracytoplasmic structures (arrows) represent negative-stained images of bacilli. For immunohistochemistry, deparaffinized sections were washed in tris-buffered saline (pH 7.4) and preincubated for 10 min with blocking buffer (0.5% albumin w/v in tris-buffered saline or nonimmune serum) to inhibit nonspecific protein binding, followed by incubation with the primary antibody. The secondary antibodies were counterstained with New Fuchsin. (**D**) HAM 56 (a macrophage-associated specific antibody) costained (pink) the ISH-positive (black grains) Langhans'-type multinucleated macrophages (arrow). (**E**) Higher magnification of Fig. 1D showing colocalization of HIV-1 signal in mononuclear (arrows) and multinucleated (arrowhead) macrophages containing acid-fast (red) bacilli (Kinyoun's stain) (original magnification, ×400).

Mycobacterium avium complex (MAC)–infected lymph nodes excised from a patient with widely disseminated disease (*10*) and analyzed by identical ISH methods demonstrated that the marked HIV-1 expression was not unique to PC infection and in fact, the HIV-1 burden was even more pronounced in the MAC-infected specimens (Fig. 1, C and D). The HIV-1 signal varied considerably among cells, from severalfold above the background level to an amount of grains that obscured the cells, and which was too numerous to resolve for the majority of cells (Fig. 2, A and B).

Immunohistochemical staining with HIV-1 p24-specific antibody paralleled the ISH results, revealing p24-positive mononuclear and multinucleated cells in the MAC- (Fig. 2C) and PC-infected specimens. In both cases, the cells producing the bulk of HIV-1 RNA were identified as mononuclear and Langhans'-type multinucleated macrophages by morphology and ISH combined with immunohistochemical staining with macrophage-associated antibodies (HAM56) (Fig. 2D) and CD68 (*11*). By sequentially performing HIV-1 ISH and staining sections with Kinyoun's stain (acid-fast), which specifically stains rod-shaped mycobacteria red, we documented that HIV-1 production occurs in both mononuclear and multinucleated giant cells that have internalized and are coinfected by MAC (Figs. 1D and 2E).

Transmission electron microscopic (TEM) analysis of PC-infected lymphoid tissue revealed cysts interspersed with inflammatory cells and remnants of PC organisms within phagocytic cells. Numerous developing, and especially, complete mature virions were readily identified by TEM (Fig. 3). In contrast, earlier studies (8), limited to OI-negative nodes, re-

vealed relatively few mature virions, and those were invariably associated with FDC processes. In these coinfected specimens, budding virions arose from the complicated plasma membranes of mononuclear and multinucleated macrophages, whereas free mature virions were concentrated around these cells, within cytoplasmic vacuoles, and dispersed in acellular areas. Although virions were found in the vicinity of lymphocytes, none were observed budding from their surfaces. Productive infection with HIV-1 did not appear to be associated with death of macrophages.

To ascertain whether this phenomenon is a general characteristic of lymphoid tissues infected with opportunistic pathogens, we compared HIV-1 production in lymph nodes with OIs from 11 HIV-1–positive subjects to a large number of HIV-1–positive, but OI-free lymph nodes. All coinfected biopsy specimens, with a single exception, had substantially greater numbers of HIV-1–expressing cells per unit area relevant to parallel analyses of non-OI lymph nodes (Table 1). Compared to non-OI lymph nodes, which possess minimal numbers of HIV-1–infected cells of monocyte/macrophage lineage, these cells become a major, but not exclusive, source of HIV-1 in the OI-infected tissues. Levels ranging from a fivefold to more than a hundredfold increase in the number of productively infected cells were consistent with OI-induced HIV-1 expression. The differences in actual HIV-1 RNA copies per cell present in the OI- and non-OI–infected tissues are actually even more notable because the density of signal in the OI-infected specimens typically precludes resolution of individual grains.

As judged by multiple parameters, the macrophage, whether infected (for example, MAC, *Mycobacterium kansasii*, *Histoplasma capsulatum*, M. *tuberculosis*) or uninfected (for example, PC) by opportunistic pathogens, can be responsible for production of large amounts of HIV-1 at the very time CD4 lymphocytes are minimal. Furthermore, the extensive viral replication by tissue macrophages provides compelling evidence that OIs can markedly change HIV-1 expression by this population of target cells. OIs apparently have the capacity to establish foci of HIV-1 production by recruitment of HIV-1–infected and infectible macrophages and stimulating their viral expression. The mechanism of up-regulation of HIV-1 RNA expression by OIs is still to be resolved (*12*, *13*).

At all stages of HIV-1 disease (from hyperplasia through involution and lymphocyte depletion) lymphoid tissues free of OIs typically display few if any HIV-1–expressing macrophages, as detected by dual ISH and immunohistochemistry (Table 1) (*7*, *13*). Nonetheless, our observations suggest that a large reservoir of such macrophages exists in the host, and that under conditions characteristic of progressive HIV-1 disease, these cells may become a major source of virus. Although the incidence and severity of OIs accelerate rapidly as the peripheral CD4 lymphocyte count falls below 200 cells per cubic millimeter (*14*), significant infections—such as M. *tuberculosis*, candida, herpes simplex virus, and herpes zoster—can occur at relatively high CD4 lymphocyte counts (*1*) and may influence HIV-1 replication in both lymphocyte and macrophage populations. Furthermore, the effect of nonopportunistic infections, such as sexually transmitted diseases, on HIV-1 viremia must also be taken into account (*15*). The influence of the OI-macrophage phenomenon on antiviral induction and maintenance therapy thus becomes a key issue.

A major impact on morbidity and mortality in HIV-1 disease has come from successful prevention and treatment of a broad range of OIs, most notably *Pneumocystis carinii* pneumonia, MAC, and cytomegalovirus. Based on our observations, controlling HIV-1 production by this means may be as significant as elimination of the direct pathogenicity of the OIs (*13*, *16*). Our findings on viral production by macrophages, together with the newly identified role of the macrophage CCR5 coreceptor on initial HIV-1 selection and infection (*17*), suggest the need for a reassessment of the overall contributions of the macrophage in HIV-1 disease and as a therapeutic target.

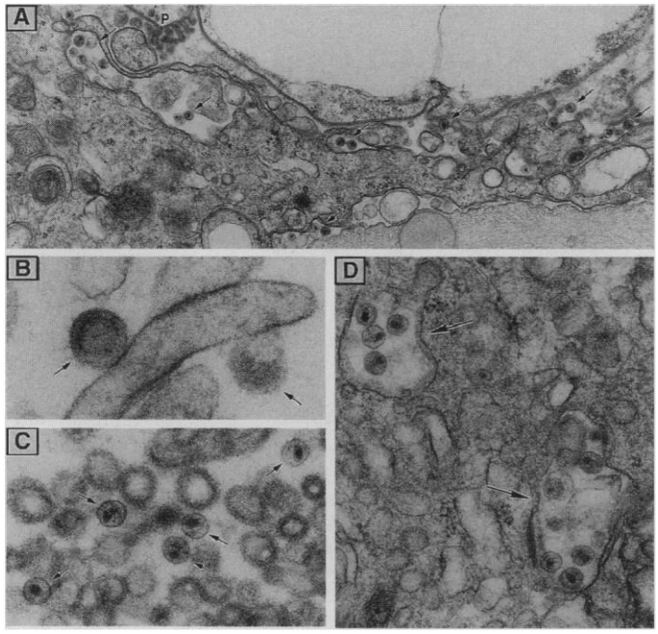

Fig. 3. HIV-1 identification in PC-infected lymph node by TEM. Glutaraldehyde-fixed surgical tissue was postfixed in OsO_4, dehydrated through graded ethanol and propylene oxide, embedded in Spurr's epoxy, and thick- and thin-sectioned. Thin sections were placed on copper grids, stained with uranyl acetate and lead citrate, and viewed in a Zeiss EM10 microscope (LEO Electron Microscopy, Thornwood, New York). (**A**) In this field, at least 20 mature HIV particles (several indicated by arrows) are associated with only a small area of a macrophage plasma membrane. The cell abuts a PC cyst (P) (original magnification, ×25,000). (**B**) Two spike-covered virions bud from a single macrophage process (arrows) (original magnification, ×130,000). (**C**) Five mature virions (arrows) are intermixed with membranous vesicles shed from PC organisms (original magnification, ×50,000). (**D**) Several mature virions are within each of two Golgi vacuoles (arrows) in the cytoplasm of a macrophage (original magnification, ×66,000).

REFERENCES AND NOTES

1. M. B. Feinberg, *Lancet* **348**, 239 (1996); A. S. Fauci, *Science* **262**, 1011 (1993).
2. M. Ghassemi *et al.*, *J. Infect. Dis.* **171**, 68 (1995); Z. Toossi, J. G. Sierra-Madero, R. A. Blinkhorn, M. A. Mettler, E. A. Rich, *J. Exp. Med.* **177**, 1511 (1993); M. C. Heng, S. Y. Heng, S. G. Allen, *Lancet* **343**, 255 (1994); M. Denis and E. Ghadiriani, *Clin. Exp. Immunol.* **97**, 76 (1994); D. Goletti *et al.*, *J. Immunol.* **157**, 1271 (1996).
3. C. Whalen *et al.*, *Am. J. Respir. Crit. Care Med.* **151**, 129 (1995).
4. E. J. Claydon, J. Bennett, D. Gor, S. M. Forster, *AIDS (London)* **5**, 113 (1991); T. Lazzarotto *et al.*, *J. Infect.* **28**, 287 (1994).
5. R. M. Donovan, C. E. Bush, N. P. Markowitz, D. Baxa, L. D. Saravolatz, *J. Infect. Dis.* **174**, 401 (1996).
6. J. Embretson *et al.*, *Nature* **362**, 359 (1993); G. Pantaleo *et al.*, *Immunol. Rev.* **140**, 104 (1994).
7. C. H. Fox *et al.*, *J. Infect. Dis.* **164**, 1051 (1991).
8. S. M. Wahl, J. M. Orenstein, P. D. Smith, *Immunology of HIV Infection*, S. Gupta, Ed. (Plenum, New York, 1996), pp. 303–336.
9. Lymphoid tissues were obtained with informed consent from a subject with Factor VIII–deficient hemophilia who had been treated with whole blood and non–heat-treated Factor VIII and was diagnosed as HIV-1–positive at age 30. He developed pentamidine-induced diabetes mellitus while a subject of a study comparing azidothymidine (AZT) versus dideoxyinosine and pentamidine, and disseminated *Pneumocystis carinii* pneumonia was diagnosed at age 34. The lymph node tissue was obtained during biospy of a nasopharyngeal mass and enlarged left cervical and jugular lymph nodes 2 years before death. Tissues were processed for light and electron microscopy.
10. Mesenteric and peripancreatic lymph nodes and

spleen were removed with informed consent from an HIV-1–positive (diagnosed 5 years earlier) 32-year-old male bisexual on AZT with a CD4 T cell count of 2, hepatosplenomegaly, and MAC infection. Lymph nodes and spleen were heavily involved with MAC and were removed 6 months before death. No additional organisms were identified. Samples of the MAC-infected lymph nodes were paraffin embedded and unavailable for TEM.
11. J. M. Orenstein *et al.*, data not shown.
12. Y. Zhang, K. Nakata, M. Weiden, W. N. Rom, *J. Clin. Invest.* **95**, 2324 (1995); G. Poli *et al.*, *Proc. Natl. Acad. Sci. U.S.A.* **87**, 782 (1990).
13. S. M. Wahl and J. M. Orenstein, *J. Leukocyte Biol.*, in press.
14. A. S. Perelson, A. U. Neumann, M. Markowitz, J. M. Leonard, D. D. Ho, *Science* **271**, 1582 (1996).
15. C. M. Magro *et al.*, *Hum. Pathol.* **27**, 1066 (1996).
16. D. P. Chin *et al.*, *J. Infect. Dis.* **170**, 578 (1994); J. W. Pape, S. S. Jean, J. L. Ho, A. Hafner, W. D. Johnson, *Lancet* **342**, 268 (1993); E. R. Cooper, B. Damon, D. Reinke, A. Caliendo, S. I. Pelton, in *4th Conference on Retroviruses and Opportunistic Infections*, Washington, DC, 22 to 26 January 1997, p. 185; C. Whalen *et al.*, *AIDS (London)* **11**, 455 (1997).
17. M. Samson *et al.*, *Nature* **382**, 722 (1996); H. K. Deng *et al.*, *ibid.* **381**, 661 (1996); T. Dragic *et al.*, *ibid.*, p. 667; G. Alkhatib *et al.*, *Science* **272**, 1955 (1996); B. Doranz *et al.*, *Cell* **85**, 1149 (1996); H. Choe *et al.*, *ibid.*, p. 1135.
18. We thank C. Rehm, S. Hoover, C. Dye III, and S. Honig for technical assistance and K. Angelis for manuscript preparation. Supported in part by NIDR contract DE12585 (J.M.O.).

5 February 1997; accepted 5 May 1997

Crystal Structure of Human BPI and Two Bound Phospholipids at 2.4 Angstrom Resolution

Lesa J. Beamer, Stephen F. Carroll, David Eisenberg*

Bactericidal/permeability-increasing protein (BPI), a potent antimicrobial protein of 456 residues, binds to and neutralizes lipopolysaccharides from the outer membrane of Gram-negative bacteria. At a resolution of 2.4 angstroms, the crystal structure of human BPI shows a boomerang-shaped molecule formed by two similar domains. Two apolar pockets on the concave surface of the boomerang each bind a molecule of phosphatidylcholine, primarily by interacting with their acyl chains; this suggests that the pockets may also bind the acyl chains of lipopolysaccharide. As a model for the related plasma lipid transfer proteins, BPI illuminates a mechanism of lipid transfer for this protein family.

The outer membrane of Gram-negative bacteria contains the complex glycolipid lipopolysaccharide (LPS) (*1*). When present in the mammalian bloodstream, LPS elicits a powerful immune response that may include fever, hypotension, multiple organ failure, and, in severe cases, septic shock and death (*2*). In mammals, two related (45% sequence identity) LPS-binding proteins have been characterized that mediate the biological effects of LPS and participate in the innate immune response to bacterial infection: LPS-binding protein (LBP) and BPI. LBP is a plasma protein that enhances the inflammatory response to LPS (*3*), whereas BPI is found in lysosomal granules of polymorphonuclear neutrophils, is bactericidal, and neutralizes the toxic effects of LPS (*4*). Recombinant NH_2-terminal fragments of BPI retain biological activity (*5*), neutralize LPS in humans (*6*), and may have clinical utility (*4*).

BPI and LBP share functional and sequence similarity with two proteins responsible for lipid transport in the mammalian bloodstream (*7*). These plasma lipid transport proteins are involved in regulating the size, shape, and composition of lipoprotein particles such as high-density lipoproteins, and are not related to structurally characterized lipid-binding proteins such as the lipocalins (*8*). Here, we present the crystal structure of BPI and two bound phospholipids at 2.4 Å resolution. Our model provides the first structural information on the LPS-binding and lipid transport protein family and suggests a common mode of lipid binding for its members.

Purified, full-length, nonglycosylated, recombinant human BPI expressed in CHO cells was crystallized by hanging drop vapor diffusion at room temperature. The protein concentration was 8.5 mg/ml and the crystallization buffer contained 12% (w/v) polyethylene glycol (molecular weight 8000), 200 mM magnesium acetate, and 100 mM sodium cacodylate (pH 6.8). Two crystal forms with slightly different cell dimensions grow under the same conditions in space group C2, with one molecule per asymmetric unit. Form 1 crystals are reproducible and have cell dimensions of a = 185.0 Å, b = 37.2 Å, c = 84.3 Å, and β = 101.3°. Form 2 crystals appear rarely and have cell dimensions of a = 185.6 Å, b = 33.0 Å, c = 85.2 Å, and β = 101.6° (Tables 1 and 2).

BPI is a boomerang-shaped molecule with approximate dimensions of 135 by 35 by 35 Å (Fig. 1, A and B). It consists of two domains of similar size (NH_2- and COOH-terminals) that are connected by a proline-rich linker of 21 residues (positions 230 to 250). The two domains form three structural units; barrels are found at each end of the protein, and a central β sheet forms an interface between the barrels. The secondary structure and topology of the two domains are similar, giving the protein pseudo-twofold symmetry.

Each barrel (residues 10 to 193 and 260 to 421) contains three common structural elements: a short α helix, a five-stranded antiparallel β sheet, and a long helix (Fig. 2A), in that order. We call these elements helix A, sheet N, and helix B in the NH_2-terminal domain and helix A′, sheet C, and helix B′ in the COOH-terminal domain. Sheets N and C have a series of β bulges that change the direction of their strands and cause a pronounced curve in the sheets. In each domain, the long helix lies along the concave face of the sheet, with the helical axis at ~60° to the strands of the β

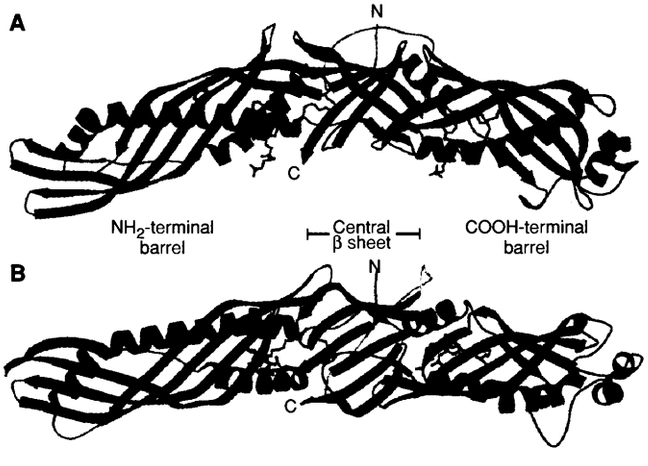

Fig. 1. (**A**) A ribbon diagram of residues 1 to 456 of BPI, illustrating its boomerang shape. The NH_2-terminal domain is shown in green, the COOH-terminal domain in blue, and the two phosphatidylcholine molecules in red. The linker is yellow, and the disulfide bond is shown as a ball-and-stick model. (**B**) View after rotating (A) 70° about the long axis of the molecule. Image produced with MOLSCRIPT (*30*) and RASTER3D (*31*).

L. J. Beamer and D. Eisenberg, UCLA-DOE Laboratory of Structural Biology and Molecular Medicine, Molecular Biology Institute, University of California, Los Angeles, CA 90095, USA.
S. F. Carroll, XOMA Corporation, 2910 Seventh Street, Berkeley, CA 94710, USA.
*To whom correspondence should be addressed.